[Poly(ethylene terephthalate) ionomer]/Silicate Hybrid Materials via Polymer–*In Situ* Sol-Gel Reactions

ALEXANDER A. LAMBERT III,[1] KENNETH A. MAURITZ,[1] DAVID A. SCHIRALDI[2]

[1] Department of Polymer Science, The University of Southern Mississippi, Hattiesburg, Mississippi 39406-0076

[2] KoSa, P.O. Box 5750, Spartanburg, South Carolina 29304-5750

Received 20 August 2001; accepted 7 September 2001

ABSTRACT: A scheme was developed for producing poly(ethylene terephthalate (PET) *ionomer*)/silicate hybrid materials via polymer–*in situ* sol-gel reactions for tetraethylorthosilicate (TEOS) using different solvents. Scanning electron microscopy/EDAX studies revealed that silicate structures existed deep within PET ionomer films that were melt pressed from silicate-incorporated resin pellets. ^{29}Si solid-state NMR spectroscopy revealed considerable Si—O—Si bond formation, but also a significant fraction of SiOH groups. ^{23}Na solid-state NMR spectra suggested the presence of ionic aggregates within the unfilled PET ionomer, and that these aggregates do not suffer major structural rearrangements by silicate incorporation. For an ionomer treated with TEOS using $MeCl_2$, Na^+ ions are less associated with each other than in the unfilled control, suggesting silicate intrusion between PET–SO_3^- Na^+ ion pair associations. The ionomer treated with TEOS + tetrachloroethane had more poorly formed ionic aggregates, which illustrates the influence of solvent type on ionic aggregation. First-scan DSC thermograms for the ionomers demonstrate an increase in crystallinity after the incorporation of silicates, but solvent-induced crystallization also appears to be operative. Second-scan DSC thermograms also suggest that the addition of silicate particles is not the only factor implicated in recrystallization, and that solvent type is important even in second-scan behavior. Silicate incorporation does not profoundly affect the second scan T_g vs. solvent type, i.e., chain mobility in the amorphous regions is not severely restricted by silicate incorporation. Recrystallization and melting in these hybrids appears to be due to an interplay between a solvent-induced crystallization that strongly depends on solvent type and interactions between PET chains and *in situ*-grown, sol-gel-derived silicate particles. © 2002 Wiley Periodicals, Inc. J Appl Polym Sci 84: 1749–1761, 2002; DOI 10.1002/app.10586

INTRODUCTION

Mauritz and coworkers have exploited the polar/nonpolar nanophase separated morphologies of perfluorosulfonate[1–6] and perfluoro(sulfonate/carboxylate)[7] ionomers such as Nafion®, elastomeric styrene-containing block copolymer ionomers, such as poly(styrene-*b*-isobutylene-*b*-styrene),[8,9] and poly(ethylene-*partially neutralized* methacrylic acid) random ionomers, such as Surlyn®,[10,11] as interactive templates that control the *in situ* sol-gel polymerizations of monomers consisting of silicon, titanium, zirconium, or aluminum alkoxides, as well as organo-alkoxysilanes, and mixtures of these tetra-, tri-, and di-functional monomers. In addition, hybrid materials based on non-

Correspondence to: K. A. Mauritz (kenneth.mauritz@usm.edu).

Contract grant sponsor: Ko Sa.

Journal of Applied Polymer Science, Vol. 84, 1749–1761 (2002)
© 2002 Wiley Periodicals, Inc.

ionomers such as poly(*n*-butyl methacrylate),[12] polyethersulfones,[13,14] and the sulfonyl fluoride precursor of Nafion®[15] have been generated in an overall effort to create novel inorganically modified polymers with enhanced properties, via polymer *in situ* sol gel processes. Regardless of the polymer/(alkoxide monomer) combination, inorganic oxide or organically modified silicate phases, having at least one nanoscopic dimension, resulted after the samples were annealed and dried of the residual alkoxide + water-compatible solvents. "Interactive," within the context of the phase-separated polymer reaction templates, refers to an energetic affinity between the hydrolyzed monomers, such as $Si(OH)_4$, and a particular domain, while "template" refers to a situation wherein the filler exclusively resides in a compatible domain.

Poly(ethylene terephthalate) (PET) ionomers can have ionic aggregates that are stabilized by strong, long-ranged Coulombic interactions. These aggregates assemble upon cooling from the melt state. Ostrowska-Czubenko and Ostrowska-Gumkowksa studied ionic interactions in the alkali metal salts, including Na^+ ionomers, of sulfonated PET using far infrared spectroscopy.[16] A band was identified that was diagnostic of the vibrations of cations in the electrostatic field of the sulfonate anions. These authors concluded that their spectroscopic data indicated that the ionic groups aggregated to form multiplets, or low-order clusters. The presence of these ionic aggregates was also suggested by the melt rheology studies of Greener et al.[17] In later studies, the ^{23}Na solid-state NMR spectroscopic studies of Boykin and Moore, of PET Na^+ form ionomers, indicate ionic aggregation.[18] This semicrystalline ionomer, shown in the structure below, incorporates a sulfonated comonomer with composition in the range of 1–10 mol %.

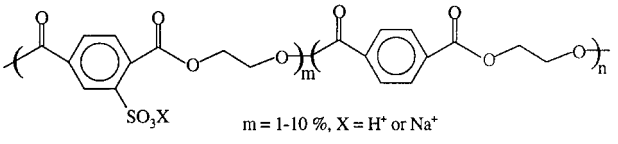

Typically, the percent crystallinity for the acid form of the ionomer is approximately 30%, whereas the sodium form of this system exhibits up to 10% crystallinity. Ostrowska-Gumkowska discusses the hindrance of crystallization in these ionomers posed by ionic aggregation and its effect on chain mobility.[19] Ostrowska-Czubenko and

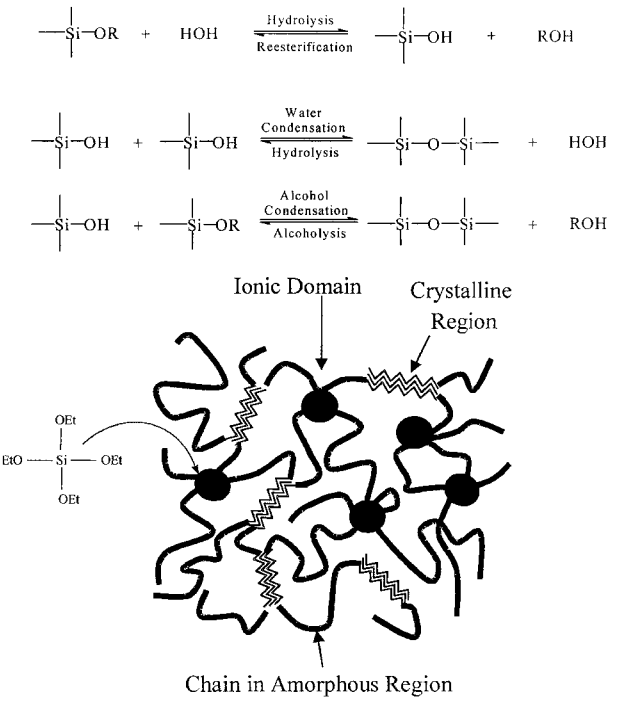

Figure 1 Sol-gel process for TEOS as being "seeded" within or around ionic aggregates in sulfonated, semicrystalline PET. It is not assumed that the silicate growths will be confined to the ionic regions.

Ostrowska-Gumkowksa also noted that, as the degree of sulfonation reaches around 10 mole %, the glass transition of K^+ form ionomers becomes broader,[20] which might be taken to reflect microstructural heterogeneity.

As described above for other polymers, these PET ionomers can be envisioned as heterogeneous media that influence the *in situ* polymerizations of sol-gel precursor monomers as well as the structure and dispersion of the resultant dried inorganic oxide phase. The hydrolysis and condensation reactions of a sol-gel process for alkoxysilane monomers that occur in a PET matrix can be envisioned as depicted in Figure 1. Although it is not assumed that the affected silicate growths are confined to the small ionic aggregate regions, it is reasonable that these domains would serve as "seed" locations in which the very polar, hydrolyzed TEOS monomers, $Si(OH)_4$, are most compatible; therefore, sol-gel reactions are most likely to initiate in such regions. Growth beyond the ionic regions would reasonably occur in the amorphous regions.

Such an intimate incorporation of nanoscopic, high surface : volume silicate particles would be expected to affect the useful properties of PET.

For example, mechanical tensile and flex moduli might be increased while thermal stability is enhanced. Although there is a disparity between the indices of refraction of silica and PET, such nanoparticles would be too small to scatter light so that the materials would exhibit optical clarity, which is an important consideration for packaging materials. Within the important arena of barrier materials, gas or liquid transport and permselectivity might be tailored not only by tortuosity considerations, but by specific interactions between the inserted silicate phase and diffusant molecules. In a somewhat related study, Turturro et al. mixed amorphous, 12 nm in size, silica particles (Cab-O-Sil) into PET.[21] It was suggested that, for appreciable loadings, there are strong interactions between the amorphous PET chain segments and the silica "nucleant" particles that lower the crystallization rate relative to unfilled PET. Hydrogen bonding between the PET carbonyl groups and ≡SiOH groups on the surfaces of the silica particles would provide strong interfacial interactions. A fundamental difference between this conventional process of dispersing preformed filler and the sol-gel process reported here is that, in the latter, the silicate phase is constructed molecule by molecule in site-specific fashion within the polymer microstructure, which is expected to lead to more intimate incorporation of nanoscopic silicate particles

Here, we report a scheme for creating such PET/silicate hybrid materials. The results of our initial characterization of their structure and properties using thermogravimetric analysis, ^{29}Si and ^{23}Na solid-state NMR spectroscopies, environmental scanning electron microscopy/energy dispersive analysis using X-rays, and differential scanning calorimetry, are described.

EXPERIMENTAL

PET Ionomers

Materials

Dimethyl terephthalate (DMT, KoSa), sodium 5-sulfoisophthalate (SIPE, E.I. DuPont Co.), ethylene glycol (EG, Celanese Co.), manganese acetate (Aldrich Co.), antimony oxide (Riedel de Haen Co.), and poly(phosphoric acid) (PPA, Rhodia Co.), of commercial grades, were used as received for the polyester melt polymerizations. Tetraethylorthosilicate (TEOS, Aldrich Co.), methylene chloride ($MeCl_2$, Fisher Co.), tetrachloroethane (TCE, Aldrich Co.), and tetrahydrofuran (THF, Fisher Co.) were used as solution components in the sol-gel polymerizations.

PET Ionomer Synthesis

PET ionomers having an intrinsic viscosity of 0.4 on the PET scale (measured as a 1% solution in dichloroacetic acid; equivalent to $M_n \sim 12{,}000$ g mol^{-1}) were produced on a 4.0 mol scale. The sulfonate comonomer composition of the ionomer used in this work was 5 mol %. For a 5 mol % copolymer of PET/SIPE, 3.8 mol of DMT and 0.2 mol of SIPE were used. For each batch, the appropriate quantity of DMT was combined with 8.8 mol of EG, 0.285 g of manganese acetate, and 0.291 g of antimony oxide, in a 2-L, 316-ss autoclave fitted with mechanical stirrer, distillation column, and gas adapter. Under ambient pressure, the reaction mixture was heated to 180–220°C, with the removal of methanol by distillation. Once the theoretical amount of methanol was removed, the desired quantity of SIPE, and 5.5 g of a 10% solution of PPA in EG were added, vacuum was slowly applied over 1 h (ultimate vacuum = 0.2 Torr), and the temperature was increased to 285°C with stirring at 10 rpm. Polymer melt viscosity was measured by means of an ammeter attached to the variable torque/fixed speed agitator motor. When the desired melt viscosity was reached, the vacuum was broken and replaced with ~2 atm pressure of dry nitrogen, and the molten polymer was extruded through an orifice at the bottom of the autoclave. The molten polymer was rapidly cooled in tap water, then ground into rough particles averaging 1–4 mm in diameter.

PET–*In Situ* Sol-Gel Reactions

The general sol-gel reaction scheme used for the incorporation of a silicate component in ionomeric PET is depicted in Figure 2. First, the ionomer pellets were dried in a vacuum oven at 100°C, for 24 h. The dried pellets were next immersed in a 5 : 1 (v/v) solvent : H_2O mixture for 24 h for various solvents. It was determined that $MeCl_2$, THF, and TCE caused the greatest ionomer swelling. Therefore, the sol-gel reaction was conducted using these carrier solvents. The water intended for alkoxide hydrolysis, as well as the solvent, also served to swell the ionomer to the extent that the permeation of hydrolyzed TEOS could take place. Next, TEOS monomer feed solutions were

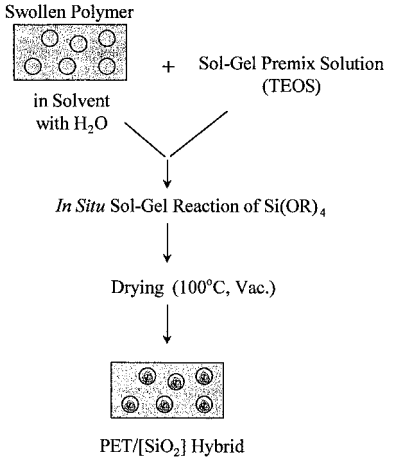

Figure 2 Sol-gel reaction scheme within a solvent + water swollen PET ionomer. Hydrolyzed TEOS molecules permeate the swollen ionomer from an external source solution.

prepared using these three solvents such that TEOS : solvent = 3 : 1 (v/v). A given TEOS solution was then added to the (same) solvent/PET ionomer swelling mixture. These three-component mixtures were agitated, and TEOS was allowed to permeate into the pellets for 24 h at room temperature. After this time, the pellets were removed from solution and annealed at 105°C in a vacuum oven for a 48 h period. This final step removes solvent and drives the internal condensation reactions between SiOH groups to a greater degree with the desired effect that the degree of intramolecular connectivity within the silicate structures is high.

Thermogravimetric Analysis (TGA)

Samples were placed into alumina crucibles and tested using a Mettler Toledo TGA850 instrument with a thermal ramp over the range 25–800°C at a 10°C/min heating rate. The percent silicate uptake was determined by subtracting the percent remaining char of the control PET ionomer from the percent char of the PET ionomer composite according to eq. (1).

$$\% \text{ silicate uptake} = \% \text{ char}_{\text{ionomer composite}} - \% \text{ char}_{\text{ionomer}} \quad (1)$$

The above analysis makes the reasonable assumption that the inorganic component will not degrade under test conditions, save for the release of an insignificant quantity of water that is generated by thermally driven condensation reactions between unreacted SiOH groups.

^{29}Si Solid-State (SS) NMR Spectroscopy

^{29}Si SSNMR spectra were acquired using a Bruker MSL-400 NMR spectrometer operating at a frequency of 79.5 MHz for ^{29}Si. A standard double air-bearing cross polarization/magic angle spinning probe was used. Samples were loaded into 4-mm fused zirconia rotors and sealed with Kel-F™ caps. Spectra were obtained using magic angle spinning with high power decoupling during acquisition only and a spinning rate of ~ 4500 Hz. A modified version of the DEPTH sequence[22] was used to suppress ^{29}Si background due to the probe. The 90° pulse width was ~4 μs, the probe dead time was 13 μs, and the acquisition time was 45 ms. The recycle delay was 180 s. All chemical shifts were referenced externally to the downfield peak of tetrakis(trimethylsilyl)silane (−9.8 with respect to TMS).

^{23}Na Solid-State (SS) NMR Spectroscopy

The ^{23}Na SSNMR measurements were also conducted on the Bruker MSL-400 instrument operating at 105.8 MHz. The external reference of a NaCl crystalline solid, which has a chemical shift of 7.1 ppm relative to the standard NaCl aqueous solution, was used to set the frequency axis. All solid samples were run in zirconia rotors using magic-angle spinning at 5 kHz and high-power proton decoupling. The samples were run with a pulse width of 1.5–2.0 μs. A pulse delay of 10 s was used to obtain fully relaxed spectra.

Scanning Electron Microscopy (SEM)/Energy Dispersive Analysis Using X-rays (EDAX)

Films for analysis were formed by melt pressing the sol-gel-modified pellets between plates that were layered with flexible sheets of polyimide release film. The films were formed with the temperature held at 260°C under a pressure of 500 psi for 10 min. The X-ray intensity of the characteristic energy for Si was divided by that of sulfur (S) to yield the relative concentration of Si as shown in eq. (2). The *S* intensity provides an internal concentration reference, being proportional to the number of sulfonate groups.

$$\text{Weighted Si to S} = \left\{ \frac{\left(\frac{\text{ATA}_{\text{Si}}}{\text{ATA}_{\text{S}}}\right)}{\left(\frac{\sum_{i=1}^{n} C_{\text{Si}_i}}{\sum_{i=1}^{n} C_{\text{S}_i}}\right)} \right\} \left\{ \frac{C_{\text{Si}_i}}{C_{\text{S}_i}} \right\} \qquad (2)$$

In this equation, the summation is over the entire film thickness, C is proportional to the X-ray intensity for the given element, and ATA is the averaged total amount of the given element.

Differential Scanning Calorimetry (DSC)

DSC analysis was performed using a Mettler DSC 30/S ThermoAnalytical device. The experiment consisted of heating the sample from 25 to 280°C at a rate of 20°C/min, followed by a rapid −350°C/min quench to −50°C to ensure that the thermal history of the sample is destroyed before rescan. The sample was then reheated to 280°C at the rate of 20°C/min and the thermal transitions recorded. The heat flow on the vertical axis is reduced to a per-gram-of-polymer basis, knowing the weight fraction of the silicate phase as determined by TGA.

RESULTS

Thermogravimetric Analysis

TGA was used to determine the percent silicate uptake of the ionomer that exists after the final drying step. TGA thermograms can also assess the thermal degradation of the PET ionomer as influenced by silicate incorporation. For example, surface groups on silicate particles might strongly interact with chemical groups on the ionomer, or extended silicate structures might envelop polymer chains so as diminish their segmental mobility.

The TGA thermograms of the PET ionomer and the TEOS-treated ionomer are shown in Figure 3. There appears to be little difference between the scan for the ionomer control sample and that of the THF-swelled, PET ionomer composite because the degradation onset temperature and remaining percent char is practically same for both. The greater weight loss for any of the TEOS-treated ionomers preceding the chemical degradation onset can be reasonably attributed to the

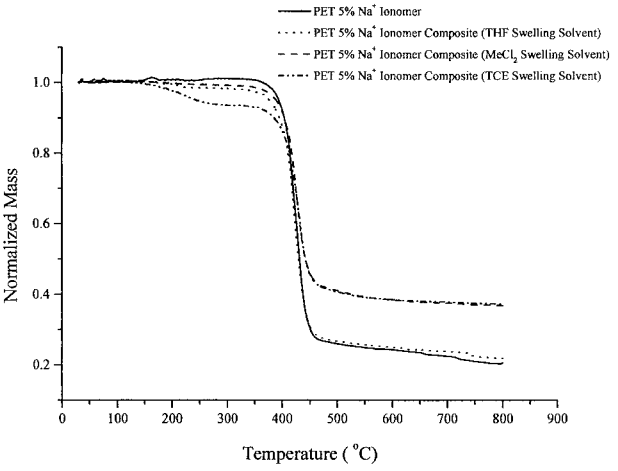

Figure 3 TGA thermograms of the unfilled PET ionomer and PET ionomers that were treated with TEOS using the three indicated carrier solvents. "Normalized mass" on the vertical axis refers to the fraction of the total mass remaining at a given temperature.

release of trapped solvent or perhaps water that is released due to secondary condensation reactions between SiOH groups that are driven by the heat supplied by the instrument. This suggests that there is little if any silicate uptake using THF as a swelling solvent, although this must be proven by more direct means. Degradation onset temperatures for the use of $MeCl_2$ and TCE solvents are similar to that of the control, which might suggest that there is little or no interaction between the silicate component and PET matrix in the sense that the former can retard the thermal degradation of the latter. The percent char for the use of these two solvents is much higher than that of the control, and there is 17% silicate uptake for both cases, which permits a meaningful comparison between the two samples. Also, for the use of TCE solvent, there is a considerable mass loss that initiates at ~150°C, which is consistent with the boiling point of TCE, thus suggesting the release of trapped solvent in this particular case.

The TGA thermograms of samples that were considered to be controls for each of the solvents are shown in Figure 4. These graphs depict the normalized (relative to 100%) solvent mass loss vs. temperature for samples swollen in each of the solvents—but without the introduction of TEOS. These samples were swollen in their respective solvent for 48 h at room temperature. The samples were then removed from the solvent and allowed to air dry before the experiment was car-

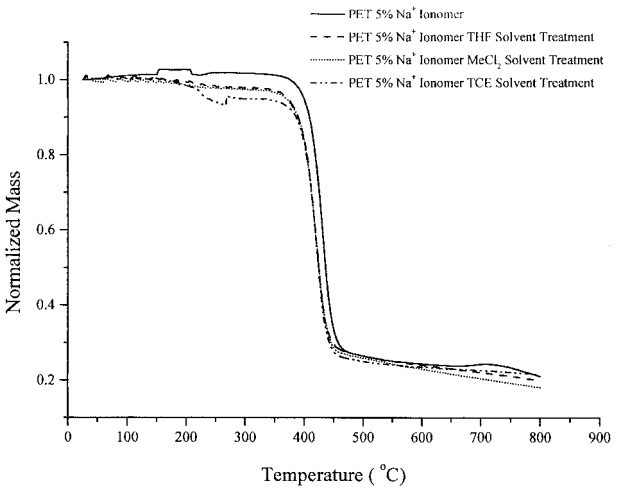

Figure 4 TGA thermograms of the PET ionomer solvent "control" samples. No silicate is present in these samples, but the pure ionomer was equilibrated in the three indicated solvents and then air dried. "Normalized mass" on the vertical axis refers to the fraction of the total mass remaining at a given temperature.

ried out. These results show that the percent char is the same for all the solvent treated systems as it is for the PET ionomer control, providing further evidence of actual silicate uptake for the ionomers using $MeCl_2$ and TCE solvents, as can be seen in Figure 3.

^{29}Si Solid-State NMR Spectroscopy

This molecular-specific probe was used to gain a measure of the degree of intramolecular connectivity of the silicate component in the same way as in other similar studies of polymer/silicate hybrid materials.[7,4,10,13,23] In amorphous silicate structures there are discrete ^{29}Si NMR peaks, each of which corresponds to the number of Si atoms that directly coordinate about the basic bonded SiO_4 tetrahedral units. The symbol Q_n designates the general coordination state $(RO)_{4-n}Si(OSi)_n$, where R can be a hydrogen atom or an alkyl group. A given Q peak is located within a characteristic range of chemical shifts relative to $Si(Me)_4$. These peak assignments fall into the following approximate ranges: $Q_1 = -85$ to -90 ppm, $Q_2 = -90$ to -95 ppm, $Q_3 = -100$ to -104 ppm, and $Q_4 = -110$ ppm.

A fundamental fact is that it is almost impossible for very small, high surface-to-volume, sol-gel-derived silicate structures to be entirely Q_4 (i.e., totally crosslinked) in character, owing to the high relative population of atoms that are forced to reside at the surfaces. The relative populations of the lower coordinated states provide a measure of uncondensed SiOH groups as well as reflect the high surface/volume aspect of the silicate structures. The relative population of a given Q state is obtained by calculating the ratio of the area under the given peak to the sum of the areas under all of the Q peaks. It is cautioned that, under the conditions of this experiment, long-ranged silicate structure is unattainable using ^{29}Si SSNMR spectroscopy in the sense of determining second and higher coordination shell structure about SiO_4 units.

Spectra for the PET ionomer/silicate (17%) composites for the cases of $MeCl_2$ and TCE solvent use are shown in Figure 5. Owing to the fact that the silicate uptakes are practically equal for these two composites, the NMR spectra can be compared in meaningful fashion. For both solvents, the chemical shift distribution indicates almost exclusively Q_3 and Q_4 coordination states with the suggestion of a slight amount of Q_2 character in the form of a shoulder on the left of each distribution. It should be appreciated that noise-to- signal for solid-state NMR samples, where the Si nuclei are diluted by a polymer matrix, can be appreciable and is expected. Nonetheless, the overall distribution that rises above the noise is in fact significant in Figure 5. The chemical shift distributions reflect silicate structures that, in a general sense, have a considerable degree of Si—

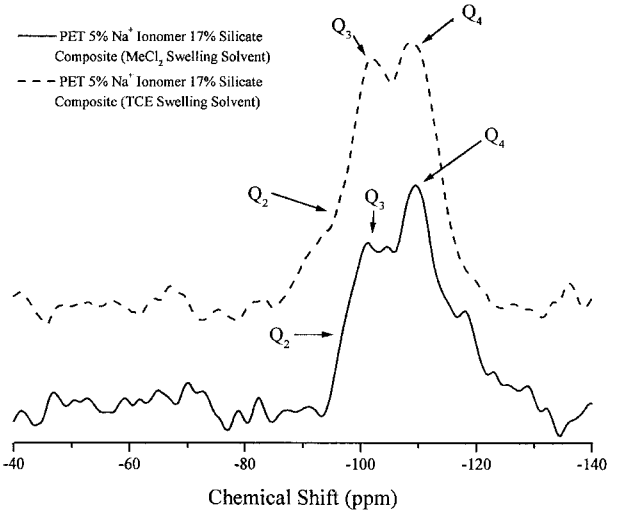

Figure 5 ^{29}Si SSNMR spectra for PET ionomer/(both 17% silicate) composites that were produced through the use of $MeCl_2$ and TCE solvents, as indicated. The approximate positions at which Q_2, Q_3, and Q_4 peaks typically occur are indicated.

O—Si bond formation while incorporating a significant fraction of uncondensed SiOH groups. Thus, *in situ* sol-gel reactions appear to have occurred.

The large population of Q_3 units, and implications with regard to the degree of the molecular interconnection of the silicate particles, implies a degree of nanoscopic porosity that is roughly depicted in Figure 6. The exact nature of this "porosity" is unknown in terms of pore size and distribution and would need to be determined by another technique. This porosity might influence the mechanical properties of these hybrids in terms of the roughness of interfacial zones and the degree to which the polymer is trapped in these pores. Also, these pores might influence the permeation of gases through these materials in the sense of molecular size exclusion, in addition to the effect of silicate particle–permeant molecule interactions and permeant molecule tortuosity posed by these dispersed inorganic obstacles.

^{23}Na Solid-State NMR Spectroscopy

^{23}Na SSNMR spectroscopy can be a sensitive probe of the immediate chemical environment and mobility of Na^+ ions owing to the interaction of the Na nuclear quadrupole moment with local electric field gradients produced by asymmetries in its electronic environment. These field gradients can be especially due to the strong electric fields posed by other Na^+ ions or to polymer-affixed anions, such as—SO_3^- groups, in the vicinity. It has been established that as peaks shift to less negative values, the interactions with Na^+ ions become weaker.[24–32] This concept can be put to use in determining whether Na^+ ions are isolated or exist in aggregates, although the absolute size of these aggregates cannot be derived from this method. Isolated sodium ions (i.e., in PET–SO_3^- Na^+ ion pairs) are characterized by a sharp peak at 7 ppm, while sodium nuclei that exist in aggregates yield a broad peak centered in the range −8 to −12 ppm, depending on the degree of ionic aggregation.

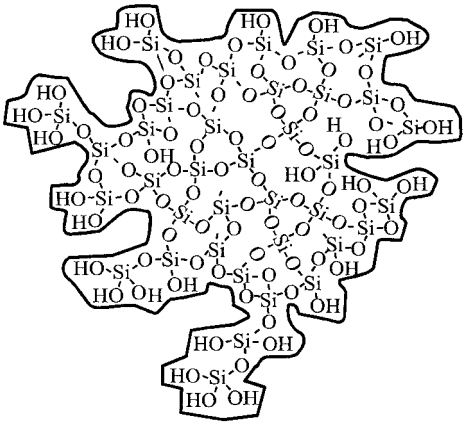

Figure 6 Rough depiction of a silicate nanoparticle having uncondensed SiOH groups that are a necessary condition for surface roughness.

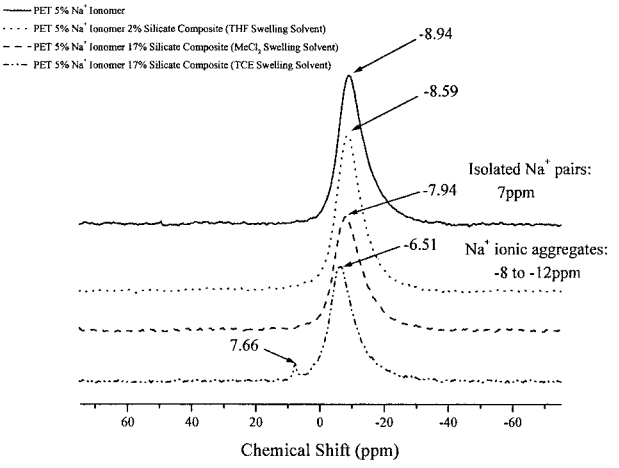

Figure 7 ^{23}Na SSNMR spectra for PET ionomer/silicate (17%) composites produced using THF, $MeCl_2$, and TCE solvents.

In the dry state, wherein ions do not have hydration shells or other strongly attached polar molecules, it is a reasonable assumption that the Na^+ ions are electrostatically bound to the polymer-affixed anions, which in these studies were charged sulfonate groups.

The ^{23}Na SSNMR spectra for the unfilled PET ionomer control and the ionomers treated with TEOS using the three solvents are shown in Figure 7. For both the control and TEOS-treated samples, the chemical shift distributions correspond to sodium nuclei that are in close proximity with each other. Despite the considerable spacing of —SO_3^- Na^+ ion pairs along the PET backbone, it appears that ion aggregates, of undetermined size, do occur in this system. This conclusion is in harmony with the evidence for ionic aggregation presented by other investigators, as discussed in the Introduction.

The unmodified control and ionomer treated with TEOS using THF have similar spectra, their chemical shifts being −8.9 and −8.6 ppm, respectively, which reflects ionic aggregation. Recall, from the above discussion of the TGA results, that

there appears to be little, if any, silicate uptake using THF as a solvent. The relatively minor perturbation on the state of Na^+ aggregation in the THF system relative to the unfilled ionomer control is in harmony with these TGA results.

For the ionomer that was treated with TEOS using $MeCl_2$, the peak is shifted to -7.9 ppm which indicates, based on prior similar studies,[28–31] that the Na^+ ions, on the average, are less associated with each other than they would be in the unfilled control. Perhaps this peak shift might be accounted for by silicate structures that, in the course of their growth, have intruded between some of the associations of PET–SO_3^- Na^+ ion pairs so as to weaken interpair interactions. This result might constitute indirect evidence of an incorporation of silicate structures within the ionic aggregate regions. Of course, the possibility that silicate structures can additionally be present in nonionic regions cannot be excluded and further structural inquiry is required in this regard. The downfield shift is distinctive—but not dramatic—and suggests that the ionic aggregates are not greatly perturbed by 17% silicate uptake.

According to the above reasoning, the ionomer treated with TEOS using TCE has ionic aggregates that are more poorly formed, as is indicated by the peak characteristic of Na^+ aggregation shifting to -6.5 ppm, and, additionally, the small peak at $+7.6$ ppm indicating isolated Na^+ ions. The spectrum of the unfilled control shows no evidence of isolated Na^+ ions so that aggregation, at least to the degree of having low-order multiplets as described in the original ionomer model of Eisenberg,[33] is a natural condition for this ionomer. The percent silicate uptake for the TCE system is the same as for the $MeCl_2$ system so that the spectroscopic differences between the two can be discussed in terms of the action of solvent molecules on ionic aggregation. The boiling point of TCE is 147°C, while that of $MeCl_2$ is much lower at 40°C. Thus, it is possible that the sample drying process removed less TCE than $MeCl_2$ in the respective experiments so that there would be a greater concentration of TCE that would interfere with ionic association in some manner.

The ^{23}Na NMR spectra of ionomers that were only swollen in each of the solvents, but without the addition of TEOS, are shown in Figure 8. The spectrum of an unfilled control ionomer which was not treated with solvent displays a peak located at -8.25 ppm that indicates Na^+ ion association. This peak shifts slightly to less association when treated with each of the solvents, although the greatest shift is not for TCE but for THF. Therefore, it would seem that solvents have the ability to change ionic association, although caution should be applied in the interpretation because rearrangements in the ionic regions might be coupled to solvent-induced rearrangements in the polymer chains.

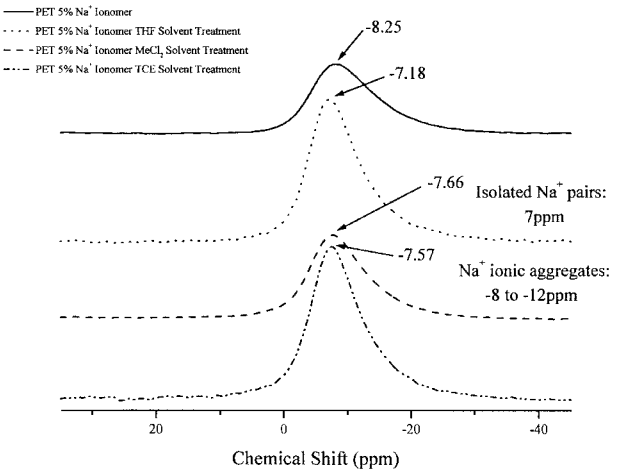

Figure 8 ^{23}Na SSNMR spectra for a PET ionomer and the PET ionomer solvent control systems.

ESEM/EDAX Analysis

EDAX was used to determine silicon elemental, and therefore, silicate compound concentration profiles across the thickness direction of the films. A general goal of these experiments was to establish whether silicate structures could be grown within the ionomer as opposed to simple, unfavorable, silicate precipitation on the film surfaces as can occur under certain conditions.

Figure 9 shows the EDAX Si elemental composition profiles across the thickness direction of ionomer/silicate composite films that were formed by melt pressing the TEOS sol-gel-modified pellets using the three solvents. The end points 0.0 and 1.0 on the horizontal axis refer to the opposite edges of the film. It is seen in these plots that there is very little incorporation of Si in the ionomer for which THF was the solvent. This is direct evidence that supports the same conclusion of no silicate incorporation based on the TGA and ^{23}Na NMR results for this same system, as discussed above. The material based on THF solvent is therefore not a composite, because it possesses essentially no internal silicate phase. For the other two composites based on $MeCl_2$ and TCE

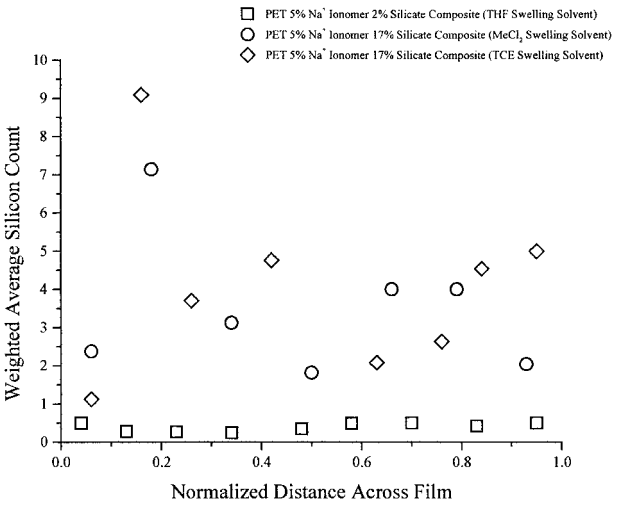

Figure 9 SEM/EDAX silicon elemental profiles across the film thickness direction for PET composites formulated using the three indicated solvents. The end points 0.0 and 1.0 on the horizontal axis refer to the edges of the film.

solvents, the plot of Si : S indicates a relatively constant and considerable concentration of Si within the film. Although some scatter exists in these data, this technique should be viewed as providing semiquantitative information regarding the presence and concentration of silicates within the interior of the film.

DSC Analysis

DSC was used to determine how silicate incorporation might influence the thermal transitions, specifically, the glass transition temperature (T_g) and melting temperature (T_m) of the PET ionomer. DSC was also used to estimate the degree of crystallinity of the PET ionomer and ionomer/silicate composites assuming that the enthalpy of melting per unit mass of the crystalline regions in the ionomer is the same as that for the crystalline regions in a PET homopolymer, i.e., ΔH_m(100% crystalline) = 135 mJ/mg.

The first scan DSC traces for the ionomer control, as well as for the three materials that were treated with TEOS using the three solvents, are shown in Figure 10. There appear to be broad crystallization exotherms followed by more distinctive melting endotherms for all systems, although the endotherm for the system derived using TCE solvent is barely perceptible. TEOS treatment increases the degree of crystallinity relative to the unfilled ionomer. Also, the glass transition becomes rather weak relative to the unfilled ionomer. The percent crystallinity of the unfilled control is estimated at 9%, based on the enthalpy of melting of unsulfonated, 100% crystalline PET, as explained above. Nine percent is a low number, but is characteristic of these copolymers having this sulfonate comonomer mol fraction.[19] In contrast, using the same DSC method, we measured an initial crystallinity of 27% for a PET homopolymer having a number average molecular weight of ~24,000 g mol^{-1}, although thermal history can cause variations in this number. The lower degree of crystallinity for the ionomer might be accounted for by frustration of chain packing by sodium sulfonate groups that act as defects and interfere with chain folding, as in the case of ion-carboxylate groups in Surlyn® ionomers.[11] Also, the kinetics of crystallization in the ionomer might be greatly retarded relative to the nonionic polymer due to strong interchain ionic interactions that reduce chain mobility in the amorphous phase. This idea is supported by the fact that Ostrowska-Gumkovska found that crystallinity decreases with increasing level of ionic groups in sulfonated PET.[19]

The THF-based system in Figure 10 has a rather high first scan degree of crystallinity (~36%). This might be explained in terms of solvent-induced crystallization (SINC) that may have occurred when the polymer was swollen in THF. SINC is a well-documented phenomenon in which interactive penetrants produce physical modifications in PET.[34–37] Moreover, SINC has been found in sulfonated PET.[38] Also, recall from a previous discussion that THF has little affect on the uptake of silicate compared to $MeCl_2$ and

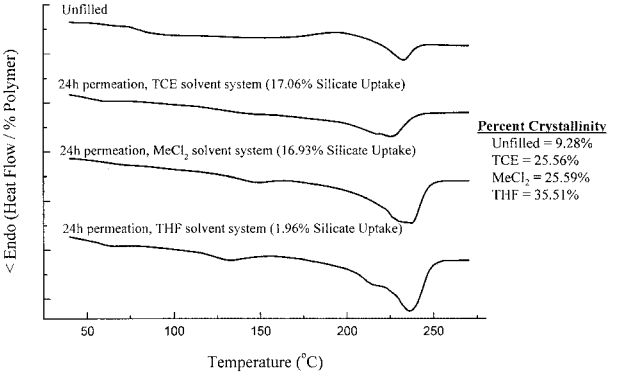

Figure 10 DSC first scans for the PET ionomer control and composites based on the use of the three different solvents. Percent crystallinities for each sample modification are indicated to the right.

TCE. Therefore, the increase in crystallinity due the action of silicate particles as heterogeneous nuclei would be limited, at best, in the case of THF solvent usage. The degree of crystallinity for both the $MeCl_2$ and TCE—based composites, as extracted from the first scan, is ~ 26%, which also might be rationalized in terms of SINC, but this crystallization must also be thought of in terms of possible interactions with silicate particles.

Each of the three TEOS-treated systems shows a two-component melting endotherm in their first scans, while the unfilled control does not. It is significant that the system that used THF in preparation exhibits dual melting, although there is no significant silicate present in the bulk regions as seen in the elemental analysis in Figure 9. Moreover, it will be seen that none of the second scans for any of the systems show two-component melting endotherms. Therefore, it seems that the presence of silicate does not account for this phenomenon, and that this is more associated with residual solvent given that these are first scans.

Dual, as well as single melting endotherms have been reported for PET homopolymers, depending on their thermal history. This phenomenon has been variously attributed to the melting of two crystal structures (e.g., chain folded structures and bundle crystals) that resided in the sample before heating,[39–43] or to partial melting of preexisting crystallites followed by recrystallization and then melting with increase in temperature.[44–46] The temperature scanning rate can also influence this phenomenon in that a single peak may appear for a fast rate but two peaks can appear when the rate is reduced.[47] Also, the solid-state polycondensation process used to prepare PET has been considered to influence melting behavior.[47] It seems that the dual melting phenomenon is not entirely understood for PET homopolymers, and less so for ionomeric variants. In any case, there is insufficient evidence here regarding the even more complex system in which sol-gel reactions have occurred to be able to reach definite mechanistic conclusions.

There appears to be a shallow, lower temperature endotherm at ~130–150°C in Figure 10 for the TEOS-treated systems using $MeCl_2$ and THF, but not for that produced using TCE. An alternate view is that this minimum merely marks the onset, or rise, of the broad crystallization exotherm that follows the prior decreasing endothermic curve section. The same curve feature is seen for the non-TEOS-treated systems in Figure 11, as will be discussed.

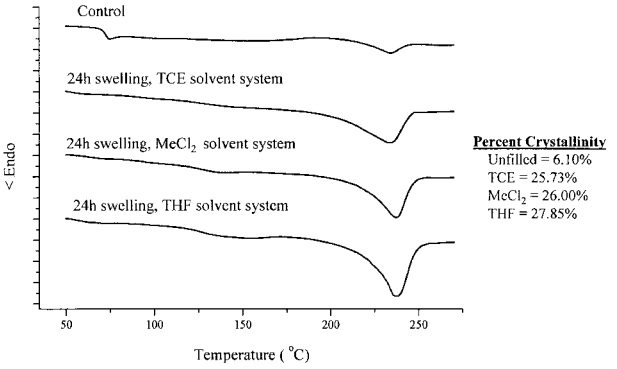

Figure 11 DSC first scans for the PET ionomer control and three solvent-treated controls. Percent crystallinities are indicated to the right.

T_g quantifies polymer chain mobility in the amorphous regions. The glass transitions in the first scan traces in Figure 10 reflect chain mobility as influenced by the history of the system. The unfilled PET ionomer shows T_g ~ 72°C while the weak glass transitions in the TEOS-treated systems have T_g ~ 62°C. Perhaps this T_g depression for the composites is due to a plasticization of the amorphous regions by solvent that is a residue of the *in situ* sol-gel process, as discussed in the results of the TGA experiments.

The first DSC scans for the dry ionomer control and the solvent-treated ionomer "control"—non-TEOS treated—are shown in Figure 11. The degrees of crystallinity of the solvent-treated systems, which are considerably higher than that of the control, are similar to those for the composites as seen in Figure 10, which would tend to support the concept of solvent-induced crystallization. Also, the melting endotherms in Figure 11 are not dual, but consist of a single peak. Figure 11 also exhibits the lower temperature feature in the range ~130–150°C in the $MeCl_2$ and THF-treated systems, but not for the system treated with TCE solvent. As will be seen on inspection of the second scans, this feature only appears on first scans. The T_g values for the solvent-treated systems are also depressed as they are for the TEOS–sol-gel-derived systems in Figure 10. Perhaps residual solvents plasticize the amorphous regions so as to impart greater chain mobility that, in turn, promotes more efficient, i.e., crystalline, chain packing.

The second scans for the unfilled ionomer control and for ionomers treated with TEOS using

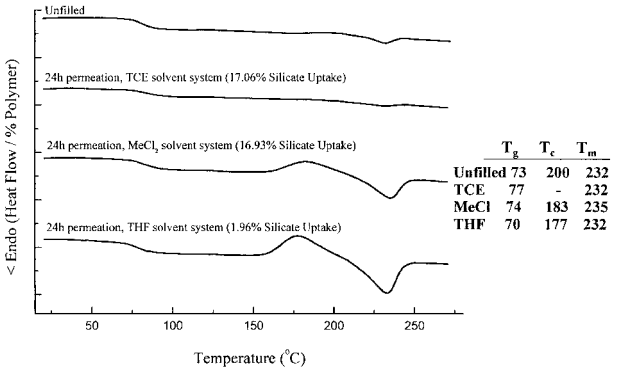

Figure 12 DSC second scan for the unfilled ionomer control and ionomers treated with TEOS for the three solvents.

the three solvents are shown in Figure 12. These scans should not be complicated by thermal activity that arises from the presence of residual solvent or by solvent release. For this reason, the glass transition appears more distinct and at higher temperatures. The incorporation of silicates does not show profound differences in the second scan T_g vs. solvent type, although its value for the use of $MeCl_2$ and TCE is somewhat higher than that for the THF case (which material, as discussed, contains little silicate) and higher than the unfilled control T_g. T_g for the TCE-based system is 7°C higher than that for the THF system, but only 4°C higher than that for the unfilled control. Chain segmental mobility in the amorphous regions does not appear to be severely is restricted by silicate incorporation in each sample.

It appears that ionic interactions retard recrystallization in the ionomer control during the time scale of the second scan experiment because a crystallization exotherm is barely visible, and the melting endotherm is weak. These features were stronger in the first scan for the control. According to Ostrowska-Gumkowska,[19] T_C is a direct measure of the crystallization rate for partially sulfonated PET ionomers, and a higher T_C is associated with slower crystallization. T_C for the unfilled control is, in fact, larger than that for the $MeCl_2$-based composite that contains a considerable silicate fraction and exhibits a distinctive crystallization exotherm as well as melting endotherm. Based on this example, it might be thought that silicate particles act as heterogeneous nucleation sites that reduce the temperature of crystallization in PET. However, the composite based on TCE, which incorporates approximately the same silicate fraction as the composite based on $MeCl_2$, shows very weak evidence of recrystallization and melting. This suggests that the addition of silicate particles is not the only factor implicated in recrystallization and that solvent type is somehow important even in second scan behavior. Furthermore, the system based on THF, which incorporates essentially no silicate in its interior, shows distinctive crystallization followed by melting, in contrast with the behavior of the unfilled control. Again, it might be concluded that the solvent is more strongly implicated in recrystallization, but that the particular behavior depends on solvent type.

The second scans for the ionomer control and solvent-treated controls (not TEOS-treated) are shown in Figure 13. The situation with regard to transition magnitude is reversed compared with that in Figure 12. The $MeCl_2$ and THF-treated systems do not display the strong recrystallization exhibited by their counterparts in Figure 12. The scan in Figure 13 for $MeCl_2$ lends support to the concept of incorporated silicate particles acting as nucleation sites but the scan for TCE does not. It is noted that T_g for all the solvent-treated systems is slightly lower than that for the control. Plasticization of the amorphous regions by residual solvent cannot be invoked owing to the fact that these are second scans.

Given the sum of this evidence, the general conclusion is that recrystallization and melting in these organic/inorganic hybrid materials is due to an interplay between solvent-induced crystallization that strongly depends on solvent type, and interactions between PET chains and *in situ*-grown, sol-gel-derived silicate particles.

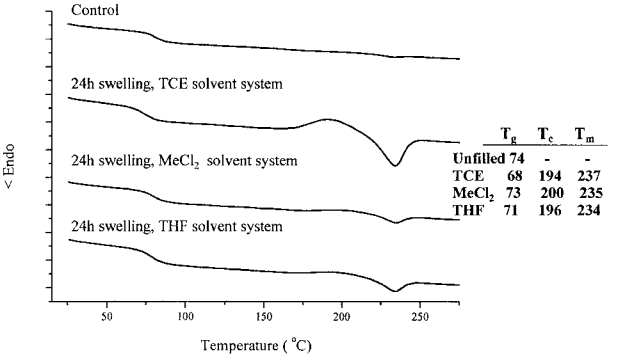

Figure 13 DSC second scans for the PET ionomer control and solvent system controls—no TEOS treatment—based on the use of the three different solvents.

CONCLUSIONS

Organic–inorganic hybrid materials were formed via PET ionomer–*in situ* sol-gel reactions for TEOS using water and different swelling solvents. ESEM/EDAX studies revealed that, after the sol-gel process and drying, silicate structures existed within melt pressed PET ionomer films, except for the case where THF is the solvent. ^{29}Si solid-state NMR spectroscopy revealed a considerable degree of Si—O—Si bond formation, although there is a significant fraction of uncondensed SiOH groups. Therefore, *in situ* sol-gel reactions successfully occurred.

^{23}Na solid-state NMR spectra suggest that ionic aggregates exist within the unfilled PET ionomer, and that these aggregates do not suffer major structural rearrangements by the incorporation of silicates into the ionomer. For the ionomer that was treated with TEOS using $MeCl_2$, it appears that Na^+ ions, on the average, are less associated with each other than they would be in the unfilled control. This suggests that evolving silicate structures have intruded between some of the PET–SO_3^- Na^+ ion pair associations. By comparison, the ionomer treated with TEOS using TCE has ionic aggregates that are more poorly formed and the spectroscopic differences, between this and the $MeCl_2$-based composite, are thought to be due to differences between the influence of different solvent molecules on ionic aggregation.

First-scan DSC thermograms for the ionomers exhibit increases in crystallinity after the incorporation of silicates. But, while silicate structures might act as heterogeneous crystallization nuclei to some degree, it appears that solvent-induced crystallization is operative, as well. Second-scan thermograms also suggest that the addition of silicate particles is not the only factor implicated in recrystallization and that solvent type is important even in second scan behavior. The incorporation of silicates does not have a profound effect on the second scan T_g vs. solvent type, suggesting that chain mobility in the amorphous regions is not severely restricted by silicate incorporation. It is concluded in a general sense that recrystallization and melting in these organic/inorganic hybrid materials is due to an interplay between solvent-induced crystallization that strongly depends on solvent type, and interactions between PET chains and *in situ*-grown, sol-gel-derived silicate particles.

The sum of the characterization evidence indicates that there is little, if any, silicate uptake using THF as a solvent, so that the resultant materials are not true organic/inorganic hybrids.

Future studies will include structural analyses of the sizes and shapes of incorporated silicate structures using transmission electron microscopy. Transient and dynamic viscoelastic properties, as influenced by PET–silicate interactions, will be investigated. Finally, gas permeation properties will be evaluated within the context of barrier materials.

The authors acknowledge the support of KoSa. We also acknowledge the assistance given in the acquisition and interpretation of the ^{29}Si and ^{23}Na SSNMR spectra by W.L. Jarrett, Department of Polymer Science, The University of Southern Mississippi.

REFERENCES

1. Deng, Q.; Moore, R. B.; Mauritz, K. A. Chem Mater 1995, 7, 2259.
2. Deng, Q.; Cable, K. M.; Moore, R. B.; Mauritz, K. A. J Polym Sci B Polym Phys Ed 1996, 34, 1917.
3. Deng, Q.; Moore, R. B.; Mauritz, K. A. J Appl Polym Sci 1998, 68, 747.
4. Shao, P. L.; Mauritz, K. A.; Moore, R. B. Chem Mater 1995, 7, 192.
5. Shao, P. L.; Mauritz, K. A.; Moore, R. B. J Polym Sci B Phys 1996, 34, 873.
6. Apichatachutapan, W.; Moore, R. B.; Mauritz, K. A. J Appl Polym Sci 1996, 62, 417.
7. Robertson, M. A. F.; Mauritz, K. A. J Polym Sci Part B Polym Phys 1998, 36, 595.
8. Reuschle, D. A.; Mountz, D. A.; Mauritz, K. A; Brister, L. B.; Storey, R. F.; Beck Tan, N. Am Chem Soc Div Polym Chem Prepr 1999, 40(2), 713.
9. Mountz, D. A.; Beck Tan, N.; Storey, R. F.; Mauritz, K. A. Am Chem Soc Div Polym Chem Prepr 2000, 41(1), 273.
10. Siuzdak, D. A.; Mauritz, K. A. J Polym Sci B Polym Phys 1999, 37, 143.
11. Siuzdak, D. A.; Start, P. R.; Mauritz, K. A. J Appl Polym Sci 2000, 77, 2832.
12. Mauritz, K. A.; Jones, C. K. J Appl Polym Sci 1990, 40, 1401.
13. Mauritz, K. A; Ju, R. Chem Mater 1994, 6, 2269.
14. Juangvanich, N.; Mauritz, K. A. J Appl Polym Sci 1998, 67, 1799.
15. Greso, A. J.; Moore, R. B.; Cable, K. M.; Jarrett, W. L.; Mauritz, K. A. Polymer 1997, 38, 1345.
16. Ostrowska-Czubenko, J.; Ostrowska-Gumkowksa, B. Eur Polym J 1988, 24, 65.
17. Greener, J.; Gillmor, J. R.; Daly, R. C. Macromolecules 1993, 26, 6416.
18. Boykin, T. L. Blends of Polyester Ionomers with Polar Polymers: Interactions, Reactions and Com-

patibilization, PhD. Dissertation, The University of Southern Mississippi, 1999.
19. Ostrowska-Gumkowska, B. Eur Polym J 1994, 30, 875.
20. Ostrowska-Czubenko, B; Ostrowska-Gumkowksa, J. Eur Polym J 1988, 24, 803.
21. Turturro, G.; Brown, G. R.; St-Pierre, L. E. Polymer 1984, 25, 659.
22. Cory, D. G.; Ritchey, W. M. J Magn Reson 1988, 80, 128.
23. Deng, Q.; Jarrett, W.; Moore, R. B.; Mauritz, K. A. J Sol-Gel Sci Technol 1996, 7, 185.
24. Komoroski, R. A.; Mauritz, K. A. J Am Chem Soc 1978, 100, 7487.
25. Samoson, A. Chem Phys Lett 1985, 119, 29.
26. Dickinson, C. L.; MacKnight, W. J.; Connolly, J. M.; Chien, C. W. Polym Bull 1987, 17, 459.
27. Park J. K.; Park, B. K.; Ryoo, R. Polym Eng Sci 1991, 31, 873.
28. O'Connell, E. M.; Root, T. W.; Cooper, S. L. Macromolecules 1994, 27, 5803.
29. O'Connell, E. M.; Root, T. W.; Cooper, S. L. Macromolecules 1995, 28, 3995.
30. O'Connell, E. M.; Root, T. W.; Cooper, S. L. Macromolecules 1995, 28, 4000.
31. O'Connell, E. M.; Peiffer, D. G.; Root, T. W.; Cooper, S. L. Macromolecules 1996, 29, 2124.
32. Orler, B. E.; Gummaraju, R. V.; Calhoun, B. H.; Moore, R. B. Macromolecules 1999, 32, 1180.
33. Eisenberg, A. Macromolecules 1970, 3, 147.
34. Durning, C. J.; Rebenfeld, L.; Russel, W. B.; Weigmann, H. D. J Polym Sci B Polym Phys 1986, 24, 1321.
35. Durning, C. J.; Rebenfeld, L.; Russel, W. B.; Weigmann, H. D. J Polym Sci B Polym Phys 1986, 24, 1341.
36. Jameel, H.; Noether, H. D.; Rebenfeld, L. J Appl Polym Sci 1982, 27, 773.
37. Jameel, H.; Noether, H. D.; Rebenfeld, L. J Appl Polym Sci 1981, 26, 1795.
38. Timm, D. A.; Hsieh, Y. J Appl Polym Sci 1994, 51, 1291.
39. Roberts, R. C. Polymer 1969, 10, 113.
40. Roberts, R. C. Polymer 1969, 10, 117.
41. Bell, J. P.; Dumbleton, J. H. J Polym Sci A-2 1969, 7, 1033.
42. Bell, J. P.; Murayama, T. J. J Polym Sci A-2 1969, 7, 1059.
43. Roberts, R. C. J Polym Sci B 1970, 8, 381.
44. Nealy, D. L.; Davis, T. G.; Kibler, C. J. J Polym Sci A-2 1970, 8, 2141.
45. Holdsworth, P. J.; Jones, T. A. Polymer 1971, 12, 195.
46. Sweet, G. E.; Bell, J. P. J Polym Sci A-2 1972, 10, 1273.
47. Qiu, G.; Tang, Z.-L.; Huang, N.-X.; Gerking, L. J Appl Polym Sci 1998, 69, 729.